

## Article

# Polyelectrolyte Platforms with Copper Nanoparticles as a Multifunctional System Aimed at Healing Process Support

Agata Lipko <sup>1</sup>, Anna Grzeczko-wicz <sup>1</sup>, Magdalena Antosiak-Iwańska <sup>1</sup>, Marcin Strawski <sup>2</sup>, Monika Drabik <sup>1</sup>, Angelika Kwiatkowska <sup>1</sup>, Ewa Godlewska <sup>1</sup> and Ludomira H. Granicka <sup>1,\*</sup>

<sup>1</sup> Nalecz Institute of Biocybernetics and Biomedical Engineering, Polish Academy of Sciences, Trojdena 4 st., 02-109 Warsaw, Poland; alipko@ibib.waw.pl (A.L.); agrzeczko-wicz@ibib.waw.pl (A.G.)

<sup>2</sup> Laboratory of Electrochemistry, Faculty of Chemistry, University of Warsaw, 00-927 Warsaw, Poland

\* Correspondence: lgranicka@ibib.waw.pl; Tel.: +48-22-592-59-00

**Abstract:** (1) Purpose: The aim of the study was to develop a nanocomposite with copper nanoparticles constituting a bacteriostatic surface to maintain human lung cell function. (2) Methods: A polyelectrolyte layer coating that incorporated copper nanoparticles was designed. As a bacteriostatic factor, copper nanoparticles were applied as a colloidal solution of copper nanoparticles (Colloid-CuNPs) and a solution of copper nanoparticles (CuNPs). The influence of the polyelectrolytes on selected Gram (+) and Gram (−) strains was examined. The function and morphology of the human adenocarcinoma A549 cell line, comprising human epithelial lung cells cultured in the presence of nanocomposite layer coatings, were evaluated. We applied fluorescence and scanning electron microscopies, as well as flow cytometry, for these studies. Furthermore, the layer coating material was characterized by atomic force microscopy (AFM) and energy dispersive X-ray analysis (EDX). (3) Results: It was observed that the polyelectrolytes polyethyleneimine (PEI) and poly-L-lysine (PLL) did not induce proliferation of the *E. coli* strain. However, they did induce the proliferation of the *S. aureus* strain. Due to the effectiveness of the CuNPs against the *E. coli* strain, CuNPs were selected for further research. The designed coatings of proper NPs shared the sustained function of human lung cells within 10 days of culture. The AFM and EDX characterization confirmed the presence of copper in the layer coating nanomaterial. The presence of CuNPs in polyethyleneimine-based nanocomposite deepened the bacteriostatic effect on *E. coli* compared with PEI alone. Meanwhile, incorporating CuNPs in PLL allowed A549 cell maintenance but did not exert a bacteriostatic influence on the examined strain. (4) Conclusions: The platform based on polyelectrolytes, incorporated with copper nanoparticles, that ensures the growth and appropriate morphology of the human lung epithelial cells, might be considered an element of a system for medical devices used to maintain the function of human lung cells.

**Keywords:** polyelectrolyte layer coating; copper nanoparticles; human lung A549 cell line



**Citation:** Lipko, A.; Grzeczko-wicz, A.; Antosiak-Iwańska, M.; Strawski, M.; Drabik, M.; Kwiatkowska, A.; Godlewska, E.; Granicka, L.H. Polyelectrolyte Platforms with Copper Nanoparticles as a Multifunctional System Aimed at Healing Process Support. *Processes* **2024**, *12*, 512. <https://doi.org/10.3390/pr12030512>

Received: 25 January 2024

Revised: 20 February 2024

Accepted: 23 February 2024

Published: 1 March 2024



**Copyright:** © 2024 by the authors. Licensee MDPI, Basel, Switzerland. This article is an open access article distributed under the terms and conditions of the Creative Commons Attribution (CC BY) license (<https://creativecommons.org/licenses/by/4.0/>).

## 1. Introduction

Scientists and engineers' efforts to construct increasingly advanced biomaterials with multifunctional profiles are reflected in the countless publications regarding new systems that support the regeneration of injured tissues and the restoration of their function [1–3]. Nonetheless, the topic remains unfathomable despite the wide range of designed and reported structures and platforms. Undoubtedly, novel biomaterials with specific properties, especially those for biomedical applications designed to meet several stringent requirements, have revolutionized modern therapy methods. However, it is worth remembering that individual patients have various physiological characteristics, making each case unique [4]. Consequently, universal biomaterials, even highly advanced ones, do not ensure the same clinical results in different patients and do not guarantee therapeutic success. An increasing number of voices suggest that the future should be associated with

personalized therapies. Therefore, in the era of the increasing popularity of personalized health care aimed at improving the quality of patients' lives, it is essential to constantly expand the base of available biomaterials intended for contact with patient tissues [4].

Antibacterial activity is a crucial property of modern biomaterials, as an element in medical device system components [5–7]. Simultaneously, the expanding antibiotic resistance of pathogens increases the demand for exploring novel antimicrobial agents and unconventional therapeutic approaches (e.g., application of antimicrobial peptide Tet213 [8] or honey [9]).

Due to their unique features, like their catalytic properties, their ability to modify surfaces to change their characteristics, and their role in energy conversion and storage, metallic nanoparticles are a novel group of nanomaterials that are usable in many areas like medicine, pharmacy, and environmental protection [10,11]. Owing to their inhibitory and robust antimicrobial effects, metal nanoparticles are recognized as an antibiotic alternative [12], circumventing multi-resistant antibacterial infections. Among the metal and metal oxide nanoparticles supporting wound healing, the most commonly applied are zinc oxide [13], iron oxide [14], cerium oxide [15], titanium oxide [16], silver [17], gold [18], and copper (CuNPs) [6]. The latter in particular have received broad attention recently as they are more accessible, eco-friendly, and cost-effective than their silver and gold equivalents [19]. Moreover, studies have shown that copper nanoparticles exhibit lower toxicity than silver nanoparticles [20,21]. Furthermore, nano-biomaterials with metallic nanoparticles, including copper-based NPs, have been developed to improve mechanical strength and involve antimicrobial activity [22]. An example of materials that are reported to show antibacterial functionality against *S. aureus* might be polyelectrolyte-copper nanocomposite coatings, with the poly(diallyldimethylammonium chloride) playing the role of a polycation, poly(sodium 4-styrenesulfonate)(PSS) used as a polyanion, and negatively charged CuNPs [23].

It is worth noting that copper nanoparticles have the ability to penetrate both viruses and bacterial cell membranes directly, liquidating them by releasing oxygen and toxic factors for the microbes. In addition, it is also a crucial living element of various human metabolic pathways. Hence, tissue regeneration can be enhanced using copper [24].

The role of coppers in angiogenesis cannot be underestimated [25–27].

The successful restoration of blood flow in injured tissues and/or the vascularization of engineered grafts, ensuring the supply of nutrients, chemicals, and oxygen, is crucial for restoring damaged areas to functional tissues; yet, it is very difficult to achieve. The cellular mechanism underlying the induction of angiogenesis by Cu is still largely unknown; however, it is currently being extensively studied [12]. Moreover, Cu has been shown to positively affect the migration and adhesion of various cell types in vitro, providing biomaterial with the ability to restore tissue continuity [28,29].

There are approaches to the usage of Cu ions for bone engineering purposes. Some authors have proposed mesoporous structured scaffolds built of bioactive glass containing CuNPs. It is true to say that the obtained structure allows for increased angiogenesis [30]. Some other authors have reported the biocompatibility of Cu<sup>2+</sup>-doped bioactive glass scaffolds for bone marrow mesenchymal stem cell maintenance and angiogenesis enhancement due to the induction of vascular endothelial growth factor secretion by Cu<sup>2+</sup> [31].

Cu ions can be used to promote angiogenesis. The 3D collagen porous scaffolds involving CuNPs were reported to be constructed for osteomyelitis treatment purposes. Along with the angiogenesis-promoting and bone-forming enhancement, an inhibitory effect on *S. aureus* was observed [32].

Copper nanoparticles are applied for bactericidal activity induction in bone cements. However, it has been observed, e.g., in the case of tested PMMA modified with copper nanoparticles, that together with the higher bactericidal effect, the pulp stem cells' viability is reduced [33].

It can be noted that Cu has been recognized as an antibacterial agent for a long time [34]. Recently, studies on different cells and organisms have established the lower cytotoxicity of

Cu nanoparticles compared to Cu ions [35]. Such results indicate that the nanoparticle form can promote the steady relatively low release of Cu ions, without reaching the activation threshold of oxidative pathways in mammals; however, they retain the ability to disrupt the integrity of bacterial cell walls and membranes. Consequently, an opportunity occurs to obtain a highly biocompatible material with antimicrobial properties. These features have also resulted in attention being paid to Cu nanoparticles in the context of bone and cartilage engineering as they exhibit remarkable pro-osteogenic and pro-chondrogenic activity [27,36,37].

As CuNPs' properties possess angiogenesis-promoting and bacteriostatic effects, their use in regeneration processes is implied.

The vital role of copper as a trace mineral required for regeneration [38] has been examined in practice. Recently, the effectiveness of commercially available dressings containing silver nanoparticles was compared with dressings containing copper nanoparticles for applications in clinical practice. It was found that the use of bandages involving copper nanoparticles enhanced the healing of hard-to-heal wounds. At the same time, bandages with copper nanoparticles proved to be more efficient than dressings containing silver nanoparticles [39].

Epithelial injury often characterizes respiratory diseases. However, an imbalance in lung homeostasis does not always lead to dysfunction. Lungs have a significant capacity to respond to injury by repairing and replacing damaged cells, with the epithelium playing a critical role in returning to homeostasis by coordinating tissue repair [40,41]. Therefore, for the components of respiratory support devices, it is advisable to develop materials that do not cause damage to epithelial cells, have bacteriostatic properties, and promote healing.

This study aims to develop a platform combining therapeutic and bacteriostatic properties as an element in the system components of medical devices to maintain the function of human lung cells.

## 2. Materials and Methods

### 2.1. Preparation of the Polyelectrolyte Layer Coatings

Copper nanopowder with particles of size 25 nm (CuNPs) (Merck/Sigma-Aldrich, Sofia, Bulgaria) and copper colloid (ColloidCuNPs) (Nano-Koloid, EU, Wielkopolskie, Poland) at a concentration of 50 ppm were used in the study.

The applied solutions were

- Copper colloid at 50 ppm from the bulk solution;
- CuNP solution at 1000 ppm, prepared from copper nanopowder and deionized water (MilliQ) with 0.1% Triton-X. The solution was sonicated in a sonication water bath for a total of 11 h at proper intervals to avoid overheating the solution.

The polyelectrolytes, poly-L-lysine hydrobromide (MW 15–30 kD) (Sigma, San Jose, CA, USA) and poly(ethyleneimine), branched, Mn ~60,000, Mw 750,000, analytical standard, 50% (*w/v*) in H<sub>2</sub>O (Sigma-Aldrich, Munchen, Germany), were applied in the study.

We designed and prepared membrane layers based on polyethyleneimine and poly-L-lysine. The primary layers, i.e., polyethyleneimine (PEI) and polylysine (PLL), were received from 1 mg/mL polyelectrolyte solutions in phosphate-buffered saline (PBS) (Biomed Lublin, Lublin, Poland). To obtain the membranes incorporating CuNPs (polyethyleneimine incorporating CuNPs (PEI-CuNPs) and polylysine incorporating CuNPs (PLL-CuNPs)), a 20 ppm or 200 ppm of CuNP water solution was added to a 1 mg/mL solution of the selected polyelectrolyte in PBS at a 1:1 ratio and stirred for 4 h at room temperature. Similarly, membranes incorporating ColloidCuNPs (i.e., polyethyleneimine incorporating ColloidCuNPs (PEI-ColloidCuNPs) and polylysine incorporating CuNPs (PLL-ColloidCuNPs)) were prepared. A bulk solution of ColloidCuNPs was added to a 1 mg/mL PBS solution of the appropriate polyelectrolyte at a 1:1 ratio, followed by stirring for 4 h at room temperature. The studied membranes are described in Table 1.

Membranes were placed on glass coverslips for evaluation in the cell-based systems.

**Table 1.** Tested membranes.

Membrane	CuNPs	ColloidCuNPs
polyethyleneimine-based		
polyethyleneimine (PEI)	No	No
polyethyleneimine incorporating CuNPs (PEI-CuNPs)	Yes	No
polyethyleneimine incorporating ColloidCuNPs (PEI-ColloidCuNPs)	No	Yes
poly-L-lysine-based		
polylysine (PLL)	No	No
polylysine incorporating CuNPs (PLL-CuNPs)	Yes	No
polylysine incorporating CuNPs (PLL-ColloidCuNPs)	No	Yes

## 2.2. Cell Culture

The media were Fetal Bovine Serum (FBS) (Sigma-Aldrich, EU, Sofia, Bulgaria) and Ham's F12 Medium/Dulbecco's Modified Eagle's Medium (F12/DMEM) (Gibco, Thermo Fisher Scientific, Waltham, MA, USA).

The human adenocarcinoma A549 cell line from a human lung was used in the reported studies. The cells were maintained in the Kaighn's Modification of Ham's F-12 Medium (F12-K medium) supplemented with 10% FBS (37 °C, 5% CO<sub>2</sub>). When the cells reached a confluence of approximately 80%, the culture bottles were emptied of the medium to wash the cells with PBS free of Ca<sup>2+</sup> and Mg<sup>2+</sup> and then trypsinize them. After trypsinization, cells (1 × 10<sup>3</sup>/cm<sup>2</sup>) were positioned on the membranes deposited on the bottom of culture wells and maintained in the culture medium for 10 days (5% CO<sub>2</sub>, 37 °C). The function of the cells was verified with propidium iodide by flow cytometry and MTT test after 3, 6, and 10 days of culture. Moreover, we employed scanning electron microscopy (SEM) to verify the immobilized cells' morphology. The cells cultured without a membrane for 10 days served as a control.

## 2.3. Cell's Functioning Evaluation

We employed flow cytometry measurements and the (3-4,5-dimethylthiazol-2-yl)-2,5-diphenyltetrazolium bromide assay (MTT) to evaluate cells' functioning and metabolic activity.

Flow cytometry analysis was performed using a Canto II flow cytometer (Becton Dickinson Immunocytometry Systems, San Jose, CA, USA) in cooperation with the software system BD FACSDiva Software v6.1.2 (Becton Dickinson, Franklin Lakes, NJ, USA).

For MTT studies, cells were deposited on the membrane films and cultured for 3, 6, and 10 days, respectively. After the specified time, the 5 g/L MTT solution was introduced to the culture in a 1:10 medium dilution, followed by 2 h of cell incubation at 37 °C with 5% CO<sub>2</sub>. Next, the solution was discarded. At the end, DMSO was added. The absorbance of a solution was measured in a spectrophotometer (HP 8452 diode-array spectrophotometer) at 550 nm after 15 min of shaking.

## 2.4. Fluorescence Staining

The cells were immobilized on the membranes, previously deposited on glass coverslips for the fluorescence staining. We fixed samples in the 4% paraformaldehyde (PFA) solution in PBS (20 °C, 15 min) for fluorescence staining. The next step was cell membrane permeabilization. TRITON X100 detergent, which allows dyes to penetrate individual cells, was employed to achieve it. After that, the fluorochrome-conjugated phalloidin (a toxin isolated from *Amanita phalloides*), which stains F-actin, was added. To visualize single cells, we added fluorochrome solution to them. In this case, the DAPI, specifically staining DNA, was applied. It should be noted that cell nuclei stained with DAPI show blue fluorescence under UV light. Finally, the samples were washed in PBS and studied using an APX1000 fluorescence microscope (Olympus). The red phalloidin fluorescence ( $\lambda = 570$  nm) and the cytoskeleton blue DAPI ( $\lambda = 460 - 500$  nm) were examined.

### 2.5. Scanning Electron Microscopy Analysis

The visualization of bacterial cells incubated in the presence of layer coatings was performed by applying scanning electron microscopy (SEM). We performed our analysis using a TM 1000 device (Hitachi, Tokyo, Japan). Firstly, bacterial cells were incubated for 24 h; then, we fixed them using 2.5% glutaraldehyde, followed by multiple rinsing with Milli Q water. Finally, the samples were placed in 75.0% ethanol for 15 min. We repeated the procedure. After that, a 15 min incubation of samples in 99.8% ethanol was performed. Next, the samples were air-dried and placed in a microscope measuring chamber.

### 2.6. SEM-EDX Studies

A Crossbeam 540X scanning electron microscope (Carl Zeiss Microscopy GmbH, Jena, Germany) with an X-FEG cathode was used for SEM-EDX characterization, whereas the X-MAXN spectrometer (Oxford Instrument, Abingdon, UK) operating at 15 keV was applied to collect the EDX maps.

It should be noted that the samples were lyophilized before entering the chamber of the microscope.

### 2.7. Statistical Analysis

Standard statistical analysis was performed by applying Statistica 7.1 software. The standard deviations, mean values, and significant differences were assessed, wherein values of  $p < 0.05$  were assumed to be significant.

## 3. Results

### 3.1. The Polyelectrolyte Layer Coatings' Bacteriostatic Effect Evaluation

The selected polyelectrolytes were examined as the base of materials for cooperation with NPs for systems aimed for medical devices to maintain human cells' function. The effect of PEI and PLL, which exhibit adhesive properties towards viruses [42], on bacterial strains of *S. aureus* and *E. coli* was examined.

It can be seen that different materials had various effects on the investigated strains. Assessing the bacteriostatic influence of the chosen polyelectrolytes demonstrated that they did not affect the Gram (+) and Gram (−) strains to the same extent. The performed assessment showed that PEI and PLL did not induce the proliferation of *E. coli*. There was no statistical difference in the optical density (OD) value between PEI and PLL ( $p = 0.065 > 0.05$ ). Additionally, the PEI had a bacteriostatic effect on *E. coli*. There was a significant difference in the optical density compared with the control ( $p = 0.016 < 0.05$ ). Furthermore, the PLL did not affect the *E. coli* strain compared with the control ( $p = 0.961 > 0.05$ ). On the other hand, it was observed that the proliferation of *S. aureus* strains was higher after incubation in the presence of the PLL and PEI polyelectrolytes (Figure 1). The *E. coli* strain, whose proliferation was not induced by the abovementioned materials, was selected for further evaluation. The lack of bacteriostatic impact on both Gram (+) and Gram (−) strains by the PLL might be caused by the weak interaction of its residues with the bacterial cell membrane.

The SEM pictures of the selected strains after a 24 h incubation in the presence of the evaluated layer coatings are presented in Figure 2.

Although the obtained optical density values indicated statistically significant differences in the proliferation of bacterial cells incubated in the presence of the coating layers, they were too small to show in the microscopic image.

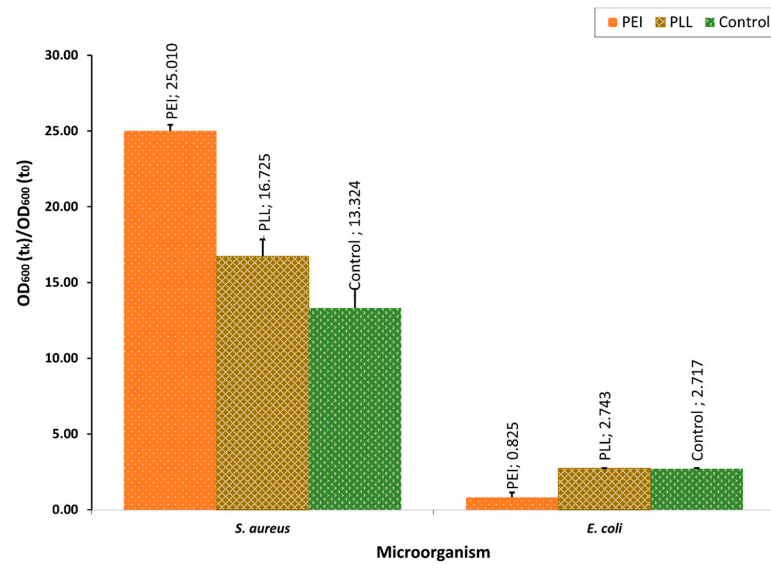


**Figure 1.** Bacterial strains' optical density. Results for *S. aureus* and *E. coli* after a 24 h culture in the presence of the polyethyleneimine (PEI) and poly-L-lysine (PLL) layer coatings are shown. The values are presented as mean  $\pm$  SD.

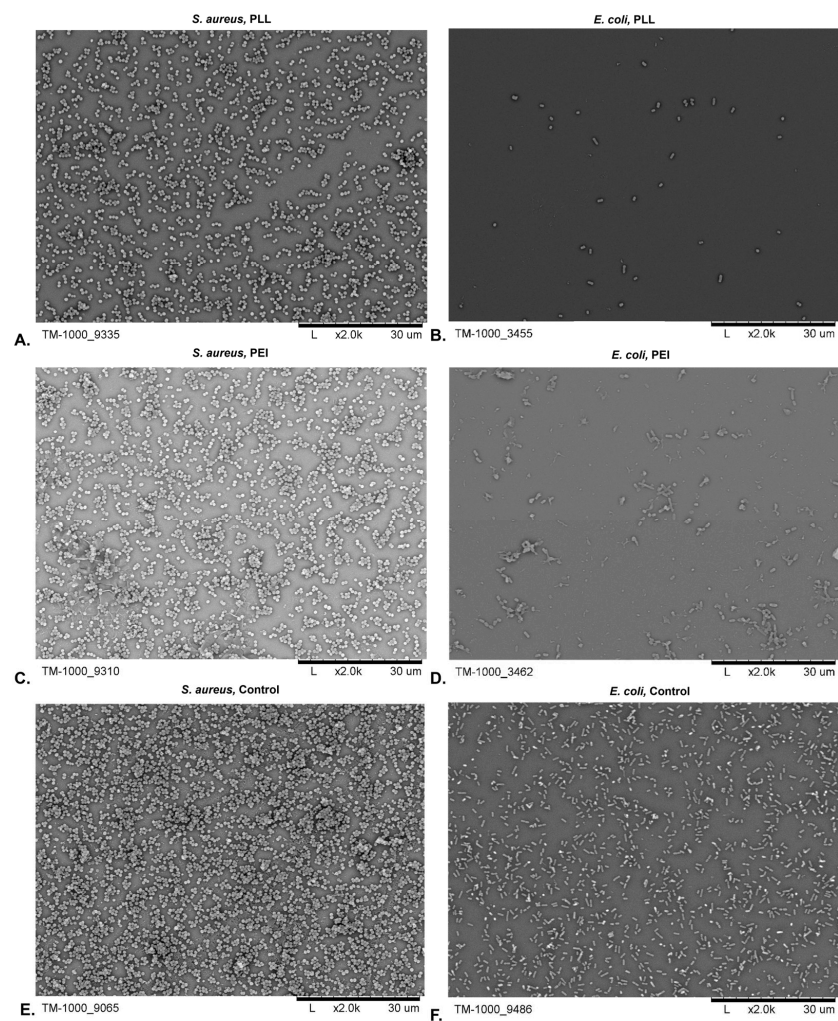


**Figure 2.** SEM picture of the strains *S. aureus* and *E. coli* after a 24 h incubation in the presence of the coating layer of PLL ((A,B), respectively), PEI ((D,E), respectively), and alone ((E,F), respectively).

### 3.2. Characterization of Polyelectrolyte Layer Coatings

Atomic forces microscopy was applied to characterize the surface morphology and topography of the nanocomposite material samples. The ColloidCuNP- or CuNP-incorporating layers were assessed. Moreover, the coating layers incorporating the chosen polyelectrolyte, PLL and PEI, nanoparticles were examined.

#### 3.2.1. Surface Topography Analysis

It can be observed that the ColloidCuNPs layer exhibited a structure with densely marked centers over the entire surface. The CuNPs layer exhibited not very dense evenly marked centers over the entire surface (Figure 3).

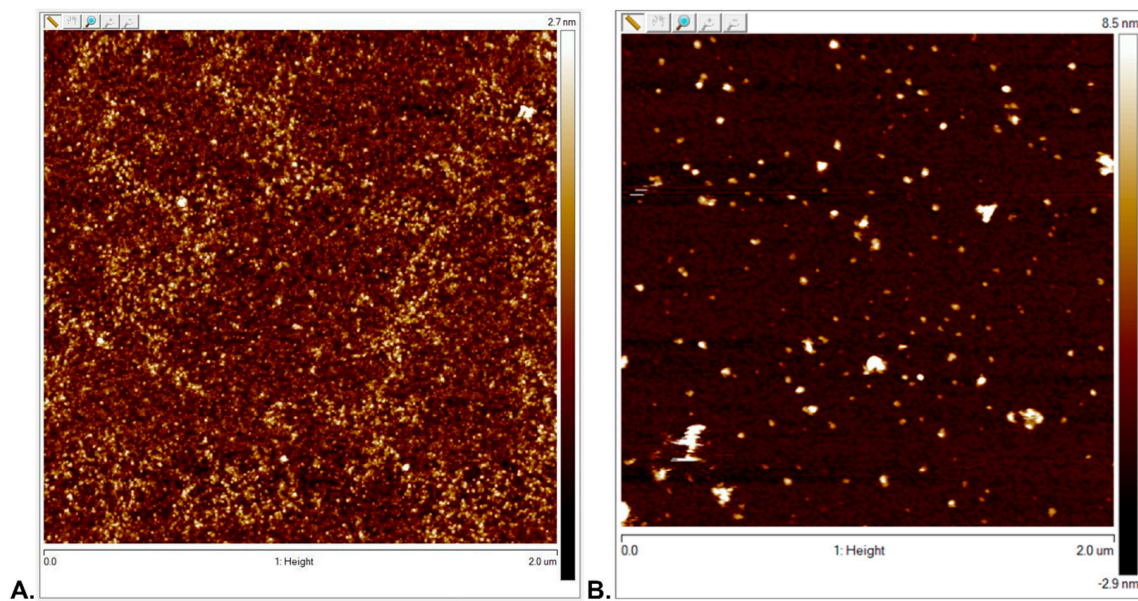


**Figure 3.** AFM visualization of the ColloidCuNPs (A) and CuNPs (B) layers. The layers were deposited on the gold mica substrate cover.

#### 3.2.2. Surface Morphology Analysis

The morphology of the layer coatings incorporating polyelectrolyte copper nanoparticles (PEI-CuNPs, PEI-ColloidCuNPs, PLL-CuNPs, and PLL-ColloidCuNPs) was assessed (Figures 4 and 5).

The PLL-ColloidCuNPs layer showed a structure with evenly marked tiny centers over the entire surface.

The PEI-ColloidCuNPs layer showed an even structure with densely distributed centers. No branched structure was observed. The PLL-ColloidCuNPs and PEI-ColloidCuNPs layers' surface maximum roughness ( $R_{max}$ ) [nm] values were 4.016 and 2.566, respectively (with a root mean square average of profile height deviations from the mean line ( $R_{ms}$ ) [nm] of 0.376 and 0.39, respectively) (Figure 4).

It was observed that the PLL-CuNPs layer exhibits a structure with evenly marked centers over the entire surface.

The PEI-CuNPs layer showed an even structure with developed active centers present, due to the branched structure of the PEI. The PLL-CuNPs and PEI-CuNPs layers'  $R_{max}$  [nm] values were 2.123 and 9.426, respectively (with a root mean square average of profile height deviations from the mean line ( $R_{ms}$ ) [nm] of 0.633 and 2.211, respectively) (Figure 5).

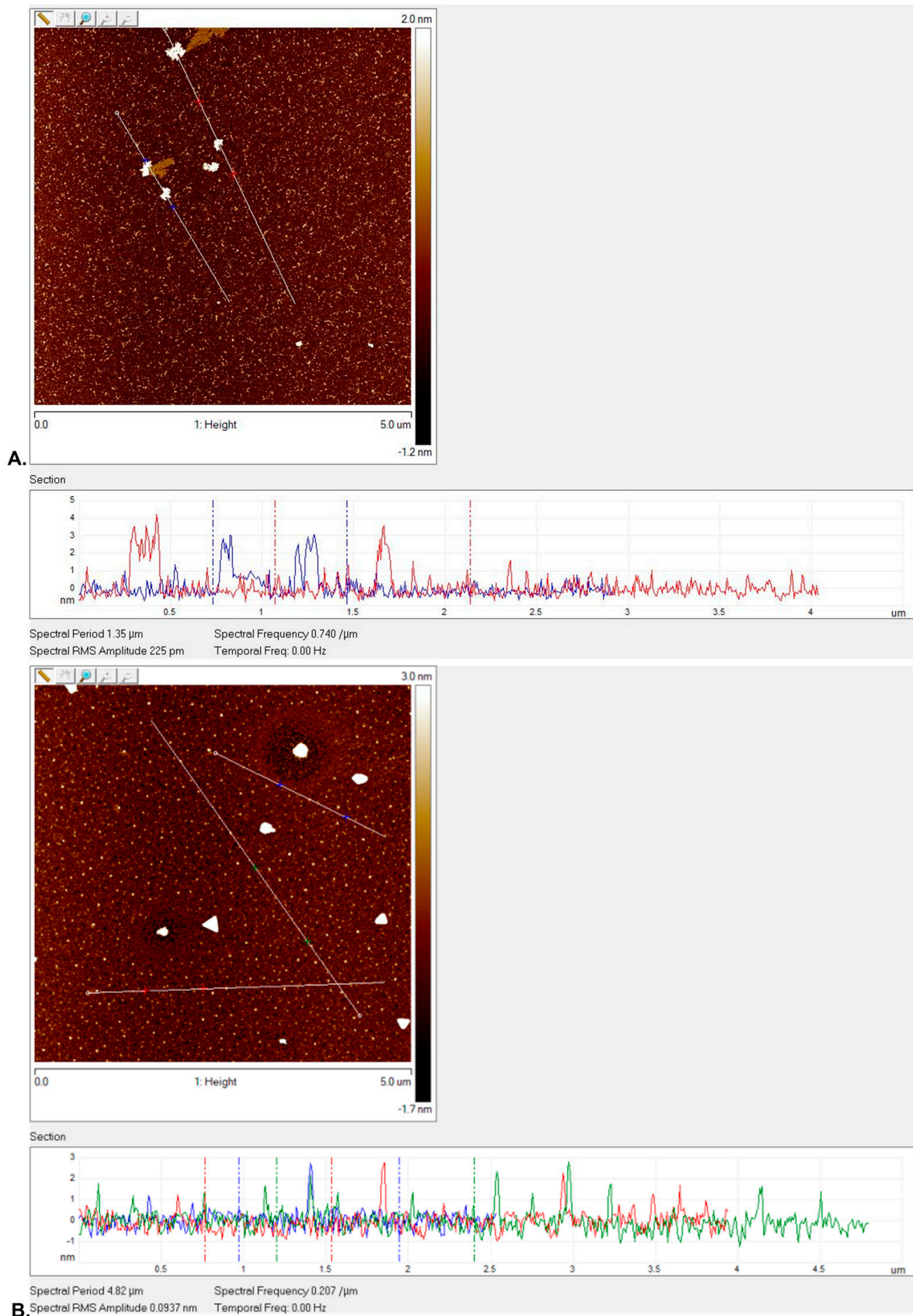


**Figure 4.** AFM visualization of the layers placed on the gold mica substrate cover. **(A)** The surface of the PLL-ColloidCuNPs coating; **(B)** the surface of PEI-ColloidCuNPs coating.

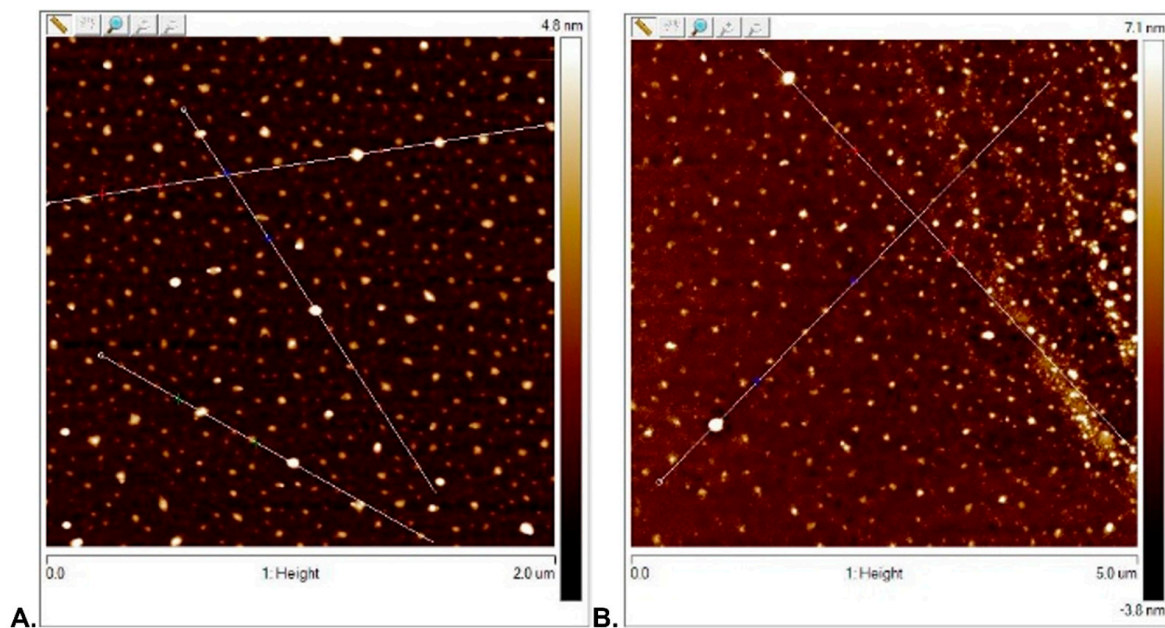


**Figure 5.** AFM visualizations present the layers deposited on the cover from the gold mica substrate. (A) The surface of the polylysine copper nanoparticles PLL-CuNPs-incorporated coating; (B) the surface of the polyethyleneimine copper nanoparticles PEI-CuNPs-incorporated coating.

### 3.3. The Copper Nanoparticles' Bacteriostatic Effect Evaluation

The bacteriostatic influence of CuNPs and ColloidCuNPs on the *E. coli* strain was assessed to examine their usability in supporting the biomaterials' bacteriostatic function (Figure 6).

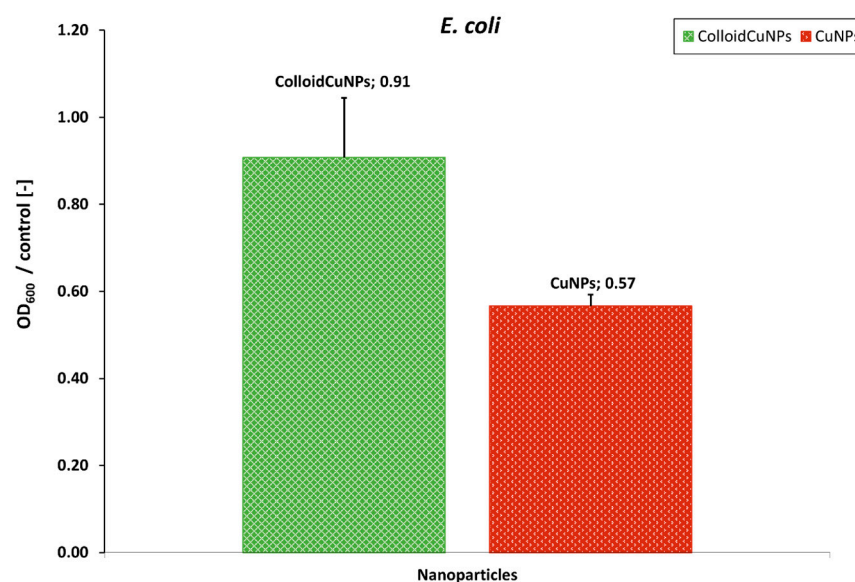


**Figure 6.** The optical density (OD) rate measured at 600 nm for the *E. coli* bacterial strain in the presence of the ColloidCuNPs and CuNPs compared to the control (*E. coli* bacterial strain cultured without additions). The values are the mean  $\pm$  SD.

A significant difference between the *E. coli* OD value for the control and the CuNPs was observed ( $p = 0.000 < 0.05$ ). Moreover, there was a significant difference between the ColloidCuNPs and CuNPs ( $p = 0.046 < 0.05$ ).

The obtained results indicated the CuNPs' bacteriostatic impact on the examined strain after a 24 h incubation. On the other hand, the ColloidCuNPs did not exert bacterio-

static influence. Thus, CuNPs were selected for further evaluation due to their apparent bacteriostatic functionality.

### 3.4. Evaluation of the CuNPs-Incorporated Layer Coatings' Performance on *E. coli*

The study of the effect on the *E. coli* strain of the PEI-CuNPs at a level enabling the maintenance of the A549 cells (presented in Section 3.6) indicates that the presence of CuNPs at a 10 ppm share in the PEI-CuNPs deepens the bacteriostatic effect compared to PEI alone ( $p = 0.034 < 0.05$ ).

On the other hand, the PLL-CuNPs did not exert a bacteriostatic influence when compared to the control ( $p = 0.148 < 0.05$ ). (Figure 7).

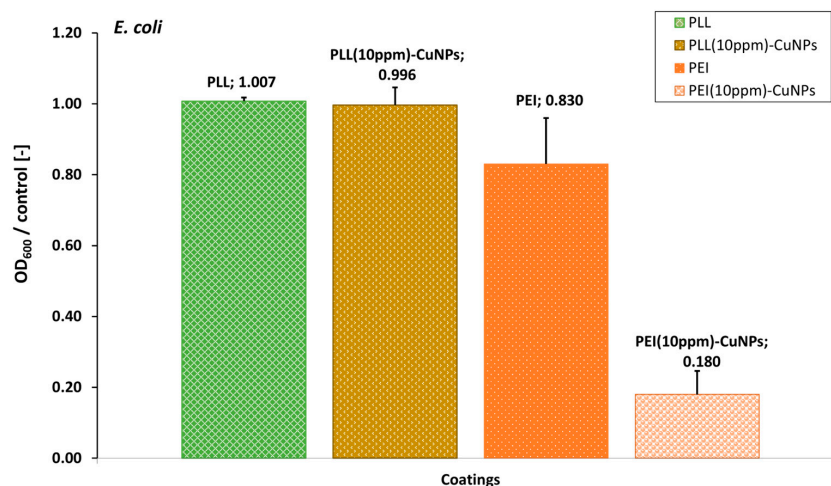


**Figure 7.** The optical density (OD) rate measured at 600 nm for the *E. coli* bacterial strain cultured in the presence of the PLL and PEI alone, as well as with the CuNPs-incorporated layer coatings relative to the control (*E. coli* bacterial strain cultured alone). The values are the mean  $\pm$  SD.

However, the overall charge of the bacterial cells at physiological pH was negative due to the presence of the carboxylic groups in the lipoproteins within the bacterial membrane [43], and the electrostatic interaction with the opposite charge of the copper ions released from nanoparticles was expected; it can be seen that the incorporation of CuNPs did not change the effect of the PEI-CuNPs on *S. aureus* (Figure 8). The influence on the *S. aureus* strains of the PEI incorporating CuNPs indicated a similar effect to that of PEI alone.

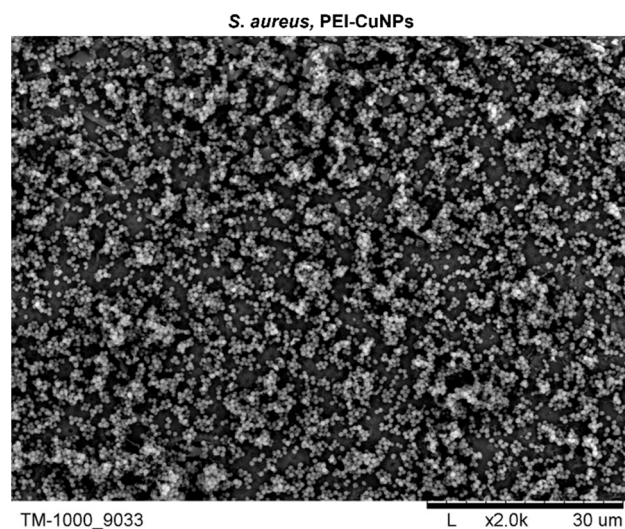


**Figure 8.** SEM image of the *S. aureus* strain after a 24 h incubation in the presence of PEI-CuNPs layer coating.

### 3.5. The CuNPs-Incorporated Polyelectrolyte Layer Coatings' Evaluation

#### 3.5.1. SEM-EDX Evaluation

Analyzing the nanocomposite material based on the PLL and PEI incorporating CuNPs, only the slight peak, which corresponded to Cu, was visible in the EDX spectra of the PEI-CuNPs and PLL-CuNPs membrane, which might be due to the overlapping polyelectrolytes signal (Figure 9).

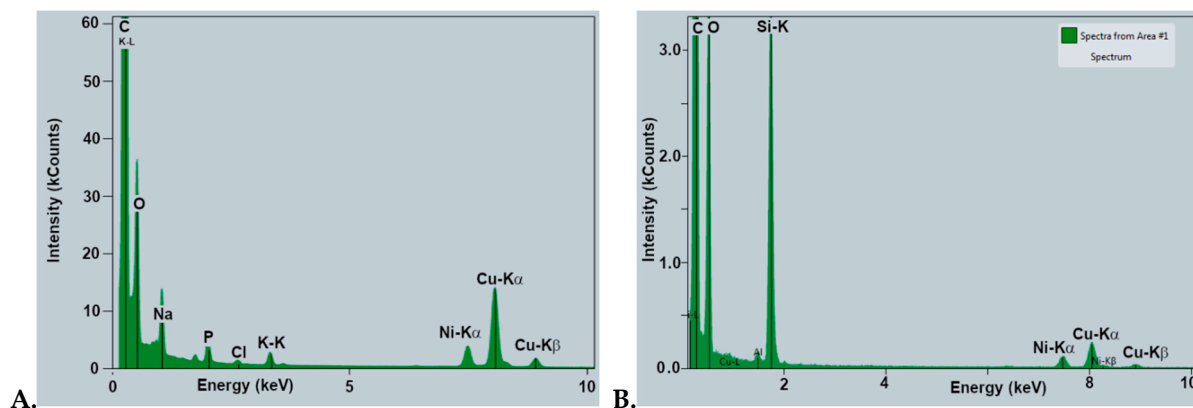


**Figure 9.** EDX spectra of PEI-CuNPs (A) and PLL-CuNPs (B) membranes with Cu peaks visible.

#### 3.5.2. Water Contact Angle Studies

The characteristics of the material surface ensure the evaluation of its potential in biomedical applications. One key analysis is hydrophilic/hydrophobic interplay [44]. The coating wettability was assessed by measuring the contact angle for water.

We tested the coatings (1) based on poly-L-lysine, polylysine 10 ppm incorporating CuNPs (PLL(10 ppm)-CuNPs), and polylysine 100 ppm incorporating CuNPs (PLL(100 ppm)-CuNPs) and (2) based on polyethyleneimine, polyethyleneimine 10 ppm incorporating CuNPs (PEI(10 ppm)-CuNPs), and polyethyleneimine 100 ppm incorporating CuNPs (PEI(100 ppm)-CuNPs).

The materials with PLL alone and incorporating CuNPs showed hydrophilic properties with an average contact angle of  $57.6 \pm 1.8$ . The materials with PEI alone and incorporating CuNPs showed hydrophilic properties with an average contact angle of  $63.2 \pm 4.42$ . There were no significant differences in the contact angle for the coatings of the primary material and the incorporation of CuNPs at different ppm.

The results can be compared as follows:

PEI with PEI(10 ppm)-CuNPs and PEI(100 ppm)-CuNPs:  $p = 0.064 > 0.05$  and  $p = 0.128 > 0.05$ , respectively;

PEI(10 ppm)-CuNPs and PEI(100 ppm)-CuNPs:  $p = 0.71 > 0.05$ ;

PLL with PLL(10 ppm)-CuNPs and PLL(100 ppm)-CuNPs:  $p = 0.436 > 0.05$  and  $p = 0.618 > 0.05$ , respectively;

PLL(10 ppm)-CuNPs with PLL(100 ppm)-CuNPs:  $p = 0.211 > 0.05$ .

Significant differences were observed when PEI was compared with PLL, PLL(10 ppm)-CuNPs, and PLL(100 ppm)-CuNPs, and the control. The results were, respectively,  $p = 0.003 < 0.05$ ,  $p = 0.002 < 0.05$ ,  $p = 0.006 < 0.05$ , and  $0.000 < 0.05$ .

No significant differences were found when PEI(10 ppm)-CuNPs were compared with PLL, PLL(10 ppm)-CuNPs, and PLL(100 ppm)-CuNPs. The results were  $p = 0.668 > 0.05$ ,  $p = 0.367 > 0.05$ , and  $p = 0.893 > 0.05$ , respectively. Furthermore, no statistically significant difference was observed between PEI(100 ppm)-CuNPs and PLL, PLL(10 ppm)-CuNPs, and PLL(100 ppm)-CuNPs. The results were, respectively,  $p = 0.331 > 0.05$ ,  $p = 0.161 > 0.05$ , and  $p = 0.701 > 0.05$ .

All the examined coatings (PEI, PEI(10 ppm)-CuNPs, PEI(100 ppm)-CuNPs, PLL, PLL(10 ppm)-CuNPs, PLL(100 ppm)-CuNPs) exhibited statistically significant differences

compared with the control (respectively,  $p = 0.000 < 0.05$ ,  $p = 0.018 < 0.05$ ,  $p = 0.003 < 0.05$ ,  $p = 0.002 < 0.05$ ,  $p = 0.034 < 0.05$ ,  $p = 0.001 < 0.05$ ). Nevertheless, as mentioned above, all the examined materials exhibited hydrophilic properties (Figure 10).

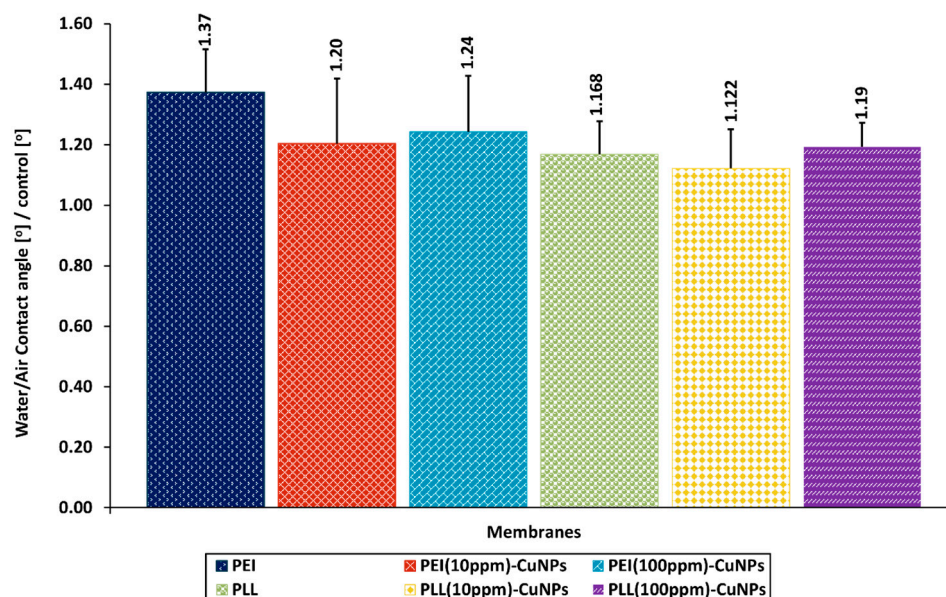


**Figure 10.** The rate of water contact angle of the layer coating surface to the control (glass surface). Key to the symbols: PLL—polylysine; PLL(10 ppm)CuNPs—polylysine incorporating 10 ppm CuNPs; PLL(100 ppm)-CuNPs—polylysine incorporating 100 ppm CuNPs; PEI—polyethyleneimine; PEI(10 ppm)-CuNPs—PEI incorporating 10 ppm CuNPs; PEI(100 ppm)-CuNPs—PEI incorporating 100 ppm CuNPs. The values are presented as mean  $\pm$  SD.

### 3.6. Evaluation of the Functioning of Human Lung Cells in the Presence of the Layer Coatings Incorporating CuNPs

#### 3.6.1. MTT Evaluation

The developed layer coatings' cytotoxicity against human lung cell lines in vitro was assessed. Cells were cultured in the presence of coatings for 10 days. The cells were maintained as a control without a coating layer present for 10 days of culture. MTT and fluorescence staining were applied to evaluate the cell function and morphology.

An MTT assay was applied to verify the mitochondrial activity of the cells cultured in the presence of the designed coatings. After a 3-day culture on the layer coatings with PLL, PLL(10 ppm)-CuNPs, and PLL(100 ppm)-CuNPs, the ratio relative to the control was comparable, and a mean of 36% of the control value was observed. There was no statistical difference between the PLL and the PLL(10 ppm)-CuNPs and PLL(100 ppm)-CuNPs (respectively,  $p = 0.211 > 0.05$ ,  $p = 0.547 > 0.05$ ) and between the PLL(10 ppm)-CuNPs and the PLL(100 ppm)-CuNPs ( $p = 0.446 > 0.05$ ).

On the other hand, after 6 days of culture, the PLL and PLL(10 ppm)-CuNPs layer coatings maintained A549 cells' function at a higher level compared with the control ( $p = 0.000 < 0.05$ ,  $p = 0.000 < 0.05$ , respectively). Moreover, on the 10th day of culture, the values obtained for the layer coatings with PLL and PLL(10 ppm)-CuNPs exhibited comparable levels with the control. Nevertheless, the values obtained for the PLL(100 ppm)-CuNPs layer coating were significantly lower than the control during the whole culture period (Figure 11).

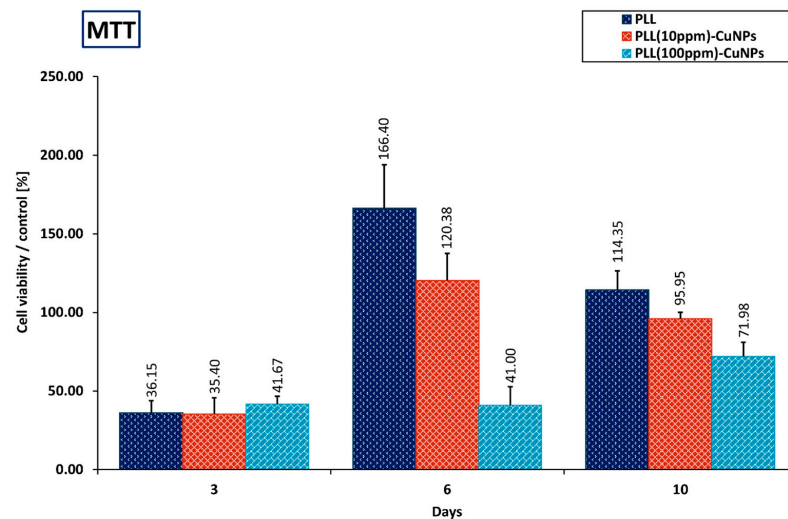


**Figure 11.** Evaluation of the mitochondrial activity of A549 cells immobilized on the PLL coating layer depicted by formazan production expressed by absorbance. The culture was maintained for 10 days. The values are presented as a ratio relative to the control (mean  $\pm$  SD). Key to the symbols: PLL—polylysine, PLL(10 ppm)-CuNPs—polylysine incorporating 10 ppm CuNPs; PLL(100 ppm)-CuNPs—polylysine incorporating 100 ppm CuNPs.

After a 3-day culture on the layer coatings with PEI, PEI(10 ppm)-CuNPs, and PEI(100 ppm)-CuNPs, the ratio relative to the control was comparable between the PEI, PEI(10 ppm)-CuNPs, and PEI(100 ppm)-CuNPs ( $p = 0.471 > 0.05$ ,  $p = 0.232 > 0.05$ , respectively), as well as between the PEI(10 ppm)-CuNPs and PEI(100 ppm)-CuNPs ( $p = 0.340 > 0.05$ ), and a mean of 45% of the control value was noted. On the contrary, after 6 days of culture, the PEI, PEI(10 ppm)-CuNPs, and PEI(100 ppm)-CuNPs layer coatings maintained A549 cells' function at a level that might become comparable to the control. On the 10th day of culture, the values of the ratio relative to the control obtained for the layer coatings with the PEI(10 ppm)-CuNPs and PEI(100 ppm)-CuNPs declined compared to the 6-day values (Figure 12).

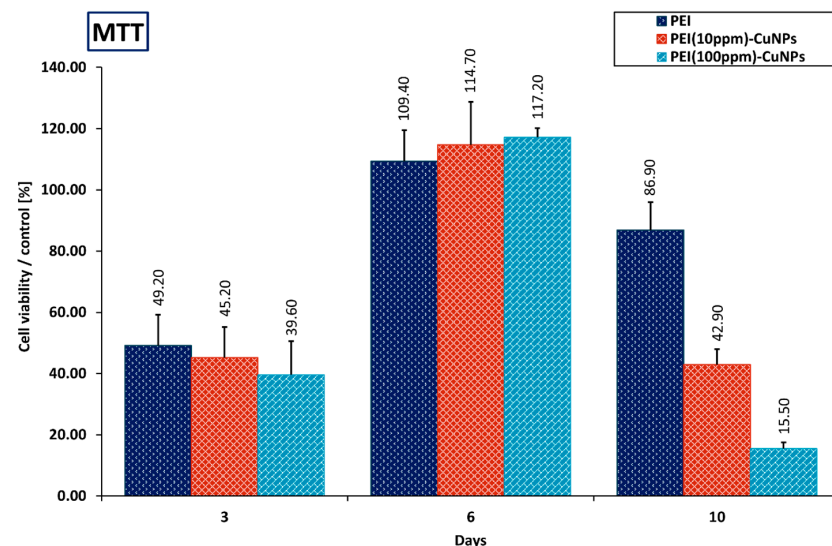


**Figure 12.** Evaluation of the mitochondrial activity of A549 cells immobilized on the PEI coating layer depicted by formazan production expressed by absorbance. The culture was maintained for 10 days. The values are presented as a ratio relative to the control (mean  $\pm$  SD). Key to the symbols: PEI—polyethyleneimine, PEI(10 ppm)-CuNPs—polyethyleneimine incorporating 10 ppm CuNPs, PEI(100 ppm)-CuNPs—polyethyleneimine incorporating 100 ppm CuNPs.

The lower mitochondrial activity values for the cultures on the layer coatings with the PLL(100 ppm)-CuNPs, PEI(100 ppm)-CuNPs, and PEI(10 ppm)-CuNPs, which became visible at different times during culture, may be the result of the enhanced ROS release due to  $\text{Cu}^{2+}$  intracellular involvement.

The obtained values indicated that the layer coatings involving CuNPs, the PEI(10 ppm)-CuNPs and PEI(100 ppm)-CuNPs coatings, maintained the A549 cells' function during the six-day culture. On the tenth day of culture, the ratio relative to the control value decreased in value. On the other hand, the PLL(10 ppm)-CuNPs coating maintained the A549 cells' function during the ten-day culture. Since the 100 ppm share induced the highest decrease, the share of 10 ppm CuNPs in the coating layer can be considered acceptable to maintain cell function.

### 3.6.2. Fluorescence Evaluation

The fluorescence microscopy evaluation performed during a week of culture showed that cells grown in the presence of PLL-CuNPs and PEI-CuNPs membranes exhibited the correct morphological structure (Figure 13). The analysis of the cells' morphology indicated spindle-shaped cells with fibroblastoid features. The numbers of cells observed on the surfaces of the glass coverslips coated with PLL-CuNPs and PEI-CuNPs were comparable. The control cells' visualization presented more numerous and clustered cells with morphology comparable to those cultured on the PLL-CuNPs and PEI-CuNPs coatings.

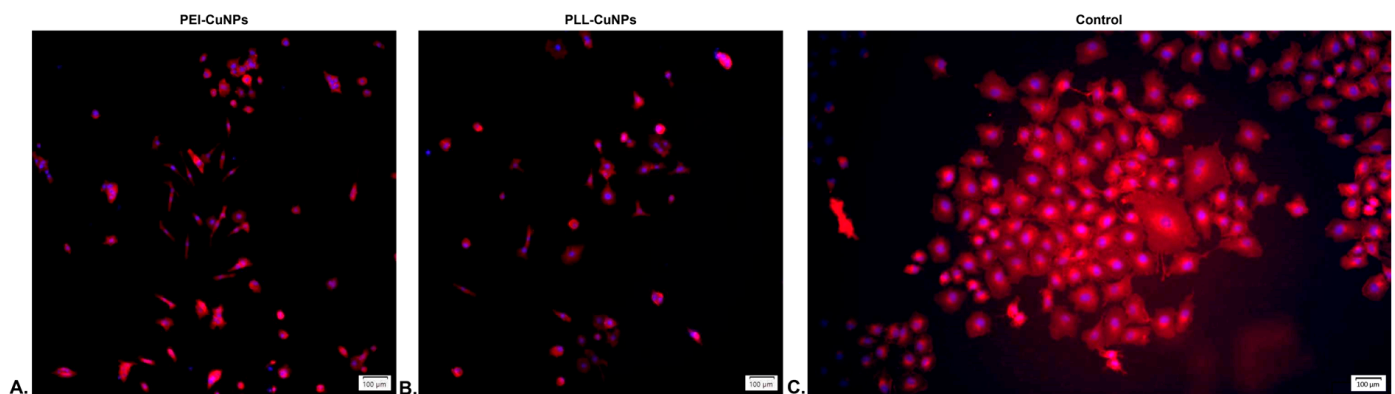


**Figure 13.** A549 cells maintained alone or in the presence of PLL(10 ppm)-CuNPs and PEI(10 ppm)-CuNPs after a week of culture. Images were obtained using fluorescence microscopy.

## 4. Discussion

Biomaterials to support processes for biomedical purposes constitute an extensive area of research, including facets of organ function preservation and tissue regeneration, antimicrobial properties, and the possibilities of bridging the gap between basic research and commercial applications.

A virus-adsorbing polyelectrolyte base material was analyzed to determine whether it also had a bacteriostatic effect against the selected Gram (+) and Gram (−) strains, and its function was verified in the configuration with incorporated copper nanoparticles.

Assuming that the isoelectric point (pI) of the spike glycoprotein for SARS-CoV-2 is equal to 6.24 [45], in the physiological environment (pH = 7.2), the stalk part is negatively charged. Consequently, positively charged groups of antiviral material could interact electrostatically with it.

Moreover, reports on Gram (−) *Escherichia coli* show that the negative charge density of the lipopolysaccharide-coated outer surface is higher than the protein surface layer of Gram (+) bacterial cells [46], which should make it much easier for such a material to adsorb Gram (−) bacterial cells.

Nevertheless, PLL did not exert a bacteriostatic effect on either Gram (+) or Gram (−) strains, which might be due to too weak of an interaction between the polylysine residues and the bacterial membrane. On the other hand, the 25 nm CuNPs in a PEI-based

nanocomposite layer coating exerted a bacteriostatic effect against *E. coli* without delimiting the A549 cells' function in the aspect of mitochondrial activity for up to a week of culture. The changes in the mitochondrial activity of cells during the 10 days of culture on the produced layer coatings may reflect the stress response induced by the involvement of the CuNPs, resulting in changes in the intra- and inter-mitochondrial redox environment; as a consequence, ROS are released. The intracellular dissolution of  $\text{Cu}^{2+}$  might enhance this effect.

Although the proposed layer coating fits into the field of biomaterials and meets specific criteria, it should be noted that an ideal biomaterial does not exist, and it is necessary to consider what the biological material is expected to cooperate with, as well as which bacterial strains it should have a bactericidal effect against. Moreover, finding a balance between the cytotoxic and bacteriostatic effects is necessary. Furthermore, it is necessary to determine the expected surface properties for individual cooperation with the intended recipient.

The size of the nanoparticles the biological material comes into contact with also plays a certain role. For example, by analyzing the toxicity of 9.2 nm copper oxide nanoparticles (CuONPs) on human bronchial epithelial cells (HBEC) as well as lung adenocarcinoma cells (A549 cells) (by applying an exposure system based on in vitro air-liquid interface), some authors observed their cytotoxic effect on cells [47].

Some other authors reported that Cu/CuO NPs of a size smaller than 20 nm suppressed the proliferation and viability of regular (WI-38) and carcinoma (A549) human lung cell lines [48].

Additionally, reports submitted for the A549 human lung cell line compared the in vitro cytotoxicity of 4 and 24 nm CuONPs [49]. The authors observed a significantly higher cytotoxicity for 24 nm CuONPs than 4 nm, which leads us to consider the balance between nanoparticle size and the NPs cell-entry extent.

The obtained results suggest that the 100 ppm share of CuNPs in the produced layer coatings excludes their use to maintain the functions of the A549 cells. The share of CuNPs in the nanocomposite coating at the level of 10 ppm allows for obtaining the balance between the cytotoxicity and bacteriostatic effect. To summarize, it is crucial to understand the antimicrobial mechanisms as separate antiviral and antibacterial functions of copper nanoparticles, considering their size and phase composition. These functions determine the potential of copper nanoparticles for biomedical purposes and may constitute a starting point for ongoing research on their use for therapeutic purposes.

## 5. Conclusions

In summary, a PEI-based layer coating containing 25 nm CuNPs at a 10 ppm share, with a topography that ensures an even contact surface for epithelial tissue cells interface and exerts a bacteriostatic effect against *E. coli* without delimiting the function of A549 cells, can be considered as an element of the system components for medical devices to maintain human lung cells' function.

**Author Contributions:** Conceptualization, A.L., A.G. and L.H.G.; methodology, A.L., A.G. and L.H.G.; validation, L.H.G.; formal analysis, L.H.G. and A.K.; investigation, A.L., A.G., M.A.-I., M.S., M.D. and E.G.; writing—original draft preparation, A.K. and L.H.G.; writing—review and editing, A.K. and L.H.G.; visualization, A.K.; supervision, L.H.G. All authors have read and agreed to the published version of the manuscript.

**Funding:** This research received no external funding.

**Data Availability Statement:** Data are contained within the article.

**Conflicts of Interest:** The authors declare no conflicts of interest.

## References

- Costa, N.N.; de Faria Lopes, L.; Ferreira, D.F.; de Prado, E.M.L.; Severi, J.A.; Resende, J.A.; de Paula Careta, F.; Ferreira, M.C.P.; Carreira, L.G.; de Souza, S.O.L.; et al. Polymeric films containing pomegranate peel extract based on PVA/starch/PAA blends for use as wound dressing: In vitro analysis and physicochemical evaluation. *Mater. Sci. Eng. C* **2020**, *109*, 110643. [[CrossRef](#)] [[PubMed](#)]
- Stricker, P.E.F.; de Souza Dobuchak, D.; Irioda, A.C.; Mogharbel, B.F.; Franco, C.R.C.; de Souza Almeida Leite, J.R.; de Araújo, A.R.; Borges, F.A.; Herculano, R.D.; de Oliveira Graeff, C.F.; et al. Human mesenchymal stem cells seeded on the natural membrane to neurospheres for cholinergic-like neurons. *Membranes* **2021**, *11*, 598. [[CrossRef](#)] [[PubMed](#)]
- Dziedzic, D.S.M.; Mogharbel, B.F.; Irioda, A.C.; Stricker, P.E.F.; Perussolo, M.C.; Franco, C.R.C.; Chang, H.W.; Abdelwahid, E.; de Carvalho, K.A.T. Adipose-Derived Stromal Cells and Mineralized Extracellular Matrix Delivery by a Human Decellularized Amniotic Membrane in Periodontal Tissue Engineering. *Membranes* **2021**, *11*, 606. [[CrossRef](#)]
- Yang, C.; Yang, C.; Chen, Y.; Liu, J.; Liu, Z.; Chen, H.J. The trends in wound management: Sensing, therapeutic treatment, and “theranostics”. *J. Sci. Adv. Mater. Devices* **2023**, *8*, 100619. [[CrossRef](#)]
- Veiga, A.S.; Schneider, J.P. Antimicrobial hydrogels for the treatment of infection. *Pept. Sci.* **2013**, *100*, 637–644. [[CrossRef](#)]
- Ponco, A.; Helmiyati, H. Hydrogel of carboxymethyl cellulose and polyvinyl alcohol modified by CuNPs as antibacterial in wound dressing. *AIP Conf. Proc.* **2020**, *2242*, 040009. [[CrossRef](#)]
- Wang, F.; Zhang, W.; Li, H.; Chen, X.; Feng, S.; Mei, Z. How Effective are Nano-Based Dressings in Diabetic Wound Healing? A Comprehensive Review of Literature. *Int. J. Nanomed.* **2022**, *17*, 2097–2119. [[CrossRef](#)]
- Annabi, N.; Rana, D.; Shirzaei Sani, E.; Portillo-Lara, R.; Gifford, J.L.; Fares, M.M.; Mithieux, S.M.; Weiss, A.S. Engineering a sprayable and elastic hydrogel adhesive with antimicrobial properties for wound healing. *Biomaterials* **2017**, *139*, 229–243. [[CrossRef](#)]
- Tashkandi, H. Honey in wound healing: An updated review. *Open Life Sci.* **2021**, *16*, 1091. [[CrossRef](#)]
- Crisan, M.C.; Teodora, M.; Lucian, M. Copper Nanoparticles: Synthesis and Characterization, Physiology, Toxicity and Antimicrobial Applications. *Appl. Sci.* **2021**, *12*, 141. [[CrossRef](#)]
- Bruna, T.; Maldonado-Bravo, F.; Jara, P.; Caro, N. Silver Nanoparticles and Their Antibacterial Applications. *Int. J. Mol. Sci.* **2021**, *22*, 7202. [[CrossRef](#)] [[PubMed](#)]
- Das, A.; Ash, D.; Fouda, A.Y.; Sudhakar, V.; Kim, Y.M.; Hou, Y.; Hudson, F.Z.; Stansfield, B.K.; Caldwell, R.B.; McMennamin, M.; et al. Cysteine oxidation of copper transporter CTR1 drives VEGFR2 signalling and angiogenesis. *Nat. Cell Biol.* **2022**, *24*, 35–50. [[CrossRef](#)] [[PubMed](#)]
- Sudheesh Kumar, P.T.; Lakshmanan, V.K.; Anilkumar, T.V.; Ramya, C.; Reshmi, P.; Unnikrishnan, A.G.; Nair, S.V.; Jayakumar, R. Flexible and microporous chitosan hydrogel/nano ZnO composite bandages for wound dressing: In vitro and in vivo evaluation. *ACS Appl. Mater. Interfaces* **2012**, *4*, 2618–2629. [[CrossRef](#)] [[PubMed](#)]
- Khashan, K.S.; Sulaiman, G.M.; Mahdi, R. Preparation of iron oxide nanoparticles-decorated carbon nanotube using laser ablation in liquid and their antimicrobial activity. *Artif. Cells Nanomed. Biotechnol.* **2017**, *45*, 1699–1709. [[CrossRef](#)] [[PubMed](#)]
- Nosrati, H.; Heydari, M.; Khodaei, M. Cerium oxide nanoparticles: Synthesis methods and applications in wound healing. *Mater. Today Bio* **2023**, *23*, 100823. [[CrossRef](#)] [[PubMed](#)]
- Kamoun, E.A.; Kenawy, E.R.S.; Chen, X. A review on polymeric hydrogel membranes for wound dressing applications: PVA-based hydrogel dressings. *J. Adv. Res.* **2017**, *8*, 217–233. [[CrossRef](#)] [[PubMed](#)]
- Vijayakumar, G.; Kim, H.J.; Rangarajulu, S.K. In Vitro Antibacterial and Wound Healing Activities Evoked by Silver Nanoparticles Synthesized through Probiotic Bacteria. *Antibiotics* **2023**, *12*, 141. [[CrossRef](#)] [[PubMed](#)]
- Soliman, W.E.; Elsewedy, H.S.; Younis, N.S.; Shinu, P.; Elsayy, L.E.; Ramadan, H.A. Evaluating Antimicrobial Activity and Wound Healing Effect of Rod-Shaped Nanoparticles. *Polymers* **2022**, *14*, 2637. [[CrossRef](#)]
- Chandrakala, V.; Aruna, V.; Angajala, G. Review on metal nanoparticles as nanocarriers: Current challenges and perspectives in drug delivery systems. *Emergent Mater.* **2022**, *5*, 1593–1615. [[CrossRef](#)]
- Ostaszewska, T.; Śliwiński, J.; Kamaszewski, M.; Sysa, P.; Chojnacki, M. Cytotoxicity of silver and copper nanoparticles on rainbow trout (*Oncorhynchus mykiss*) hepatocytes. *Environ. Sci. Pollut. Res.* **2018**, *25*, 908–915. [[CrossRef](#)]
- Salvo, J.; Sandoval, C.; Schencke, C.; Acevedo, F.; del Sol, M. Healing Effect of a Nano-Functionalized Medical-Grade Honey for the Treatment of Infected Wounds. *Pharmaceutics* **2023**, *15*, 2187. [[CrossRef](#)] [[PubMed](#)]
- Deokar, A.R.; Perelshtein, I.; Saibene, M.; Perkash, N.; Mantecchia, P.; Nitzan, Y.; Gedanken, A. Antibacterial and In Vivo Studies of a Green, One-Pot Preparation of Copper/Zinc Oxide Nanoparticle-Coated Bandages. *Membranes* **2021**, *11*, 462. [[CrossRef](#)]
- Kruk, T.; Gołda-Cępa, M.; Szczepanowicz, K.; Szyk-Warszyńska, L.; Brzywczy-Włoch, M.; Kotarba, A.; Warszyński, P. Nanocomposite multifunctional polyelectrolyte thin films with copper nanoparticles as the antimicrobial coatings. *Colloids Surf. B. Biointerfaces* **2019**, *181*, 112–118. [[CrossRef](#)] [[PubMed](#)]
- Wang, Y.; Zhang, W.; Yao, Q. Copper-based biomaterials for bone and cartilage tissue engineering. *J. Orthop. Transl.* **2021**, *29*, 60–71. [[CrossRef](#)] [[PubMed](#)]
- Xie, H.; Kang, Y. Role of copper in angiogenesis and its medicinal implications. *Curr. Med. Chem.* **2009**, *16*, 1304–1314. [[CrossRef](#)] [[PubMed](#)]
- Zhou, W.; Zi, L.; Cen, Y.; You, C.; Tian, M. Copper Sulfide Nanoparticles-Incorporated Hyaluronic Acid Injectable Hydrogel With Enhanced Angiogenesis to Promote Wound Healing. *Front. Bioeng. Biotechnol.* **2020**, *8*, 543970. [[CrossRef](#)] [[PubMed](#)]

27. Tripathi, A.; Saravanan, S.; Pattnaik, S.; Moorthi, A.; Partridge, N.C.; Selvamurugan, N. Bio-composite scaffolds containing chitosan/nano-hydroxyapatite/nano-copper-zinc for bone tissue engineering. *Int. J. Biol. Macromol.* **2012**, *50*, 294–299. [[CrossRef](#)]
28. Liu, C.; Fu, X.; Pan, H.; Wan, P.; Wang, L.; Tan, L.; Wang, K.; Zhao, Y.; Yang, K.; Chu, P.K. Biodegradable Mg-Cu alloys with enhanced osteogenesis, angiogenesis, and long-lasting antibacterial effects. *Sci. Rep.* **2016**, *6*, 27374. [[CrossRef](#)]
29. Alizadeh, S.; Seyedalipour, B.; Shafieyan, S.; Kheime, A.; Mohammadi, P.; Aghdami, N. Copper nanoparticles promote rapid wound healing in acute full thickness defect via acceleration of skin cell migration, proliferation, and neovascularization. *Biochem. Biophys. Res. Commun.* **2019**, *517*, 684–690. [[CrossRef](#)]
30. Wu, C.; Zhou, Y.; Xu, M.; Han, P.; Chen, L.; Chang, J.; Xiao, Y. Copper-containing mesoporous bioactive glass scaffolds with multifunctional properties of angiogenesis capacity, osteostimulation and antibacterial activity. *Biomaterials* **2013**, *34*, 422–433. [[CrossRef](#)]
31. Rath, S.N.; Brandl, A.; Hiller, D.; Hoppe, A.; Gbureck, U.; Horch, R.E.; Boccaccini, A.R.; Kneser, U. Bioactive Copper-Doped Glass Scaffolds Can Stimulate Endothelial Cells in Co-Culture in Combination with Mesenchymal Stem Cells. *PLoS ONE* **2014**, *9*, e113319. [[CrossRef](#)] [[PubMed](#)]
32. Ryan, E.J.; Ryan, A.J.; González-Vázquez, A.; Philippart, A.; Ciraldo, F.E.; Hobbs, C.; Nicolosi, V.; Boccaccini, A.R.; Kearney, C.J.; O'Brien, F.J. Collagen scaffolds functionalised with copper-eluting bioactive glass reduce infection and enhance osteogenesis and angiogenesis both in vitro and in vivo. *Biomaterials* **2019**, *197*, 405–416. [[CrossRef](#)] [[PubMed](#)]
33. Miola, M.; Cochis, A.; Kumar, A.; Arciola, C.R.; Rimondini, L.; Verné, E. Copper-Doped Bioactive Glass as Filler for PMMA-Based Bone Cements: Morphological, Mechanical, Reactivity, and Preliminary Antibacterial Characterization. *Materials* **2018**, *11*, 961. [[CrossRef](#)] [[PubMed](#)]
34. Grass, G.; Rensing, C.; Solioz, M. Metallic copper as an antimicrobial surface. *Appl. Environ. Microbiol.* **2011**, *77*, 1541–1547. [[CrossRef](#)] [[PubMed](#)]
35. Ameh, T.; Sayes, C.M. The potential exposure and hazards of copper nanoparticles: A review. *Environ. Toxicol. Pharmacol.* **2019**, *71*, 103220. [[CrossRef](#)] [[PubMed](#)]
36. Lin, R.; Deng, C.; Li, X.; Liu, Y.; Zhang, M.; Qin, C.; Yao, Q.; Wang, L.; Wu, C. Copper-incorporated bioactive glass-ceramics inducing anti-inflammatory phenotype and regeneration of cartilage/bone interface. *Theranostics* **2019**, *9*, 6300–6313. [[CrossRef](#)] [[PubMed](#)]
37. Kumari, S.; Mishra, A.; Singh, D.; Li, C.; Srivastava, P. In-Vitro Studies on Copper Nanoparticles and Nano-hydroxyapatite Infused Biopolymeric Composite Scaffolds for Bone Bioengineering Applications. *Biotechnol. Bioprocess Eng.* **2023**, *28*, 162–180. [[CrossRef](#)]
38. Kornblatt, A.P.; Nicoletti, V.G.; Travaglia, A. The neglected role of copper ions in wound healing. *J. Inorg. Biochem.* **2016**, *161*, 1–8. [[CrossRef](#)]
39. Gorel, O.; Hamuda, M.; Feldman, I.; Kucyn-Gabovich, I. Enhanced healing of wounds that responded poorly to silver dressing by copper wound dressings: Prospective single arm treatment study. *Health Sci. Rep.* **2024**, *7*, e1816. [[CrossRef](#)]
40. Kotton, D.N.; Morrisey, E.E. Lung regeneration: Mechanisms, applications and emerging stem cell populations. *Nat. Med.* **2014**, *20*, 822–832. [[CrossRef](#)]
41. Lucchini, A.C.; Gachanja, N.N.; Rossi, A.G.; Dorward, D.A.; Lucas, C.D. Epithelial Cells and Inflammation in Pulmonary Wound Repair. *Cells* **2021**, *10*, 339. [[CrossRef](#)] [[PubMed](#)]
42. Grzeczkwicz, A.; Lipko, A.; Kwiatkowska, A.; Strawski, M.; Baçal, P.; Więckowska, A.; Granicka, L.H. Polyelectrolyte Membrane Nanocoatings Aimed at Personal Protective and Medical Equipment Surfaces to Reduce Coronavirus Spreading. *Membranes* **2022**, *12*, 946. [[CrossRef](#)] [[PubMed](#)]
43. Corsaro, C.; Mallamace, D.; Neri, G.; Fazio, E. Hydrophilicity and hydrophobicity: Key aspects for biomedical and technological purposes. *Phys. A Stat. Mech. Its Appl.* **2021**, *580*, 126189. [[CrossRef](#)]
44. Stoimenov, P.K.; Klinger, R.L.; Marchin, G.L.; Klabunde, K.J. Metal Oxide Nanoparticles as Bactericidal Agents. *Langmuir* **2002**, *18*, 6679–6686. [[CrossRef](#)]
45. Scheller, C.; Krebs, F.; Minkner, R.; Astner, I.; Gil-Moles, M.; Wätzig, H. Physicochemical properties of SARS-CoV-2 for drug targeting, virus inactivation and attenuation, vaccine formulation and quality control. *Electrophoresis* **2020**, *41*, 1137–1151. [[CrossRef](#)] [[PubMed](#)]
46. Wilhelm, M.J.; Sharifian Gh, M.; Wu, T.; Li, Y.; Chang, C.M.; Ma, J.; Dai, H.L. Determination of bacterial surface charge density via saturation of adsorbed ions. *Biophys. J.* **2021**, *120*, 2461–2470. [[CrossRef](#)] [[PubMed](#)]
47. Jing, X.; Park, J.H.; Peters, T.M.; Thorne, P.S. Toxicity of copper oxide nanoparticles in lung epithelial cells exposed at the air-liquid interface compared with in vivo assessment. *Toxicol. Vitro.* **2015**, *29*, 502–511. [[CrossRef](#)]
48. Fahmy, H.M.; Ebrahim, N.M.; Gaber, M.H. In-Vitro evaluation of copper/copper oxide nanoparticles cytotoxicity and genotoxicity in normal and cancer lung cell lines. *J. Trace Elem. Med. Biol.* **2020**, *60*, 126481. [[CrossRef](#)]
49. Wongrakpanich, A.; Mudunkotuwa, I.A.; Geary, S.M.; Morris, A.S.; Mapuskar, K.A.; Spitz, D.R.; Grassian, V.H.; Salem, A.K. Size-dependent cytotoxicity of copper oxide nanoparticles in lung epithelial cells. *Environ. Sci. Nano* **2016**, *3*, 365–374. [[CrossRef](#)]

**Disclaimer/Publisher's Note:** The statements, opinions and data contained in all publications are solely those of the individual author(s) and contributor(s) and not of MDPI and/or the editor(s). MDPI and/or the editor(s) disclaim responsibility for any injury to people or property resulting from any ideas, methods, instructions or products referred to in the content.